Superresolving, artifact-free optical coherence tomography with deconvolution-random phase modulation

Xin Ge,[1] Si Chen,[1] Kan Lin,[1] Guangming Ni,[3] En Bo,[1] Lulu Wang,[1] and Linbo Liu[1,2*]

[1]School of Electrical and Electronic Engineering, Nanyang Technological University, Singapore 639798, Republic of Singapore

[2]School of Chemical and Biomedical Engineering, Nanyang Technological University, Singapore 637459, Republic of Singapore

[3]School of Optoelectronic Science and Engineering, University of Electronic Science and Technology of China, Chengdu 610054, China

[*]Correspondence: liulinbo@ntu.edu.sg (L. L.)

To demonstrate the superresolving performance of the Deconv-RPM method in the high-resolution image, a 20X objective lens (M Plan Apo NIR 20X, Mitutoyo, Takatsu-ku, Kawasaki, JP) was employed in the sample arm and all of 3 SLDs (Superlum Broadlighters cBLMD-T-850-HP, Ireland) were turned on. The spatial resolution of μ-OCT is 2.40 μm × 1.38 μm (*x*, *z*) in air. The system's performance was characterized by the full width at half-maximum (FWHM) of polystyrene calibration spheres (80177, Fluka, diameter 2 μm) in water with a refractive index of 1.58 at 850 nm. Paired high reflectivity signals come from the changes in the refractive index (RI) on the top and bottom edges between spheres and water. The width and spacing of the paired signals are depended on the cross-

section of the sphere that is cut through by the incident light. In the out-of-focus region, the paired signals become widen due to the broaden transverse point spread function (PSF). Supplementary Figure 1a, 1b and 1c show the logarithmic images with two-step processing. As expected, ringing artifects occur after Lucy-Richardson deconvolution (Supplementary Figure 1b) and are suppressed by the random phase masks (Supplementary Figure 1c). Gaussian kernels used in deconvolution here are fixed but not adaptive, derived from the theoretical spatial resolution. It should be noted that, some of the weak signals are suppressed by RPM in the meantime as the signal-to-noise (SNR) of image decreases in the deconvolution. Consider the confocal region only, Deconv-RPM achieves 2.8 ± 0.2 times finer lateral FWHM and 2.9 ± 0.5 times finer axial FWHM than conventional OCT. Two regions marked in Supplementary Figure 1a and 1c were enlarged to compare the resolving ability before and after Deconv-RPM processing. Two close spheres with four reflective signals are clearly resolvable in the Deconv-RPM image but entirely blurred in the conventional image (Supplementary Figure 1d). Even in the end of the depth range, separable reflective signals from merged ones suggest much superior in resolutions archived by the Deconv-RPM method. The corresponding line profiles across reflective signals before and after Deconv-RPM processing are shown in Supplementary Figure 1f and 1g.

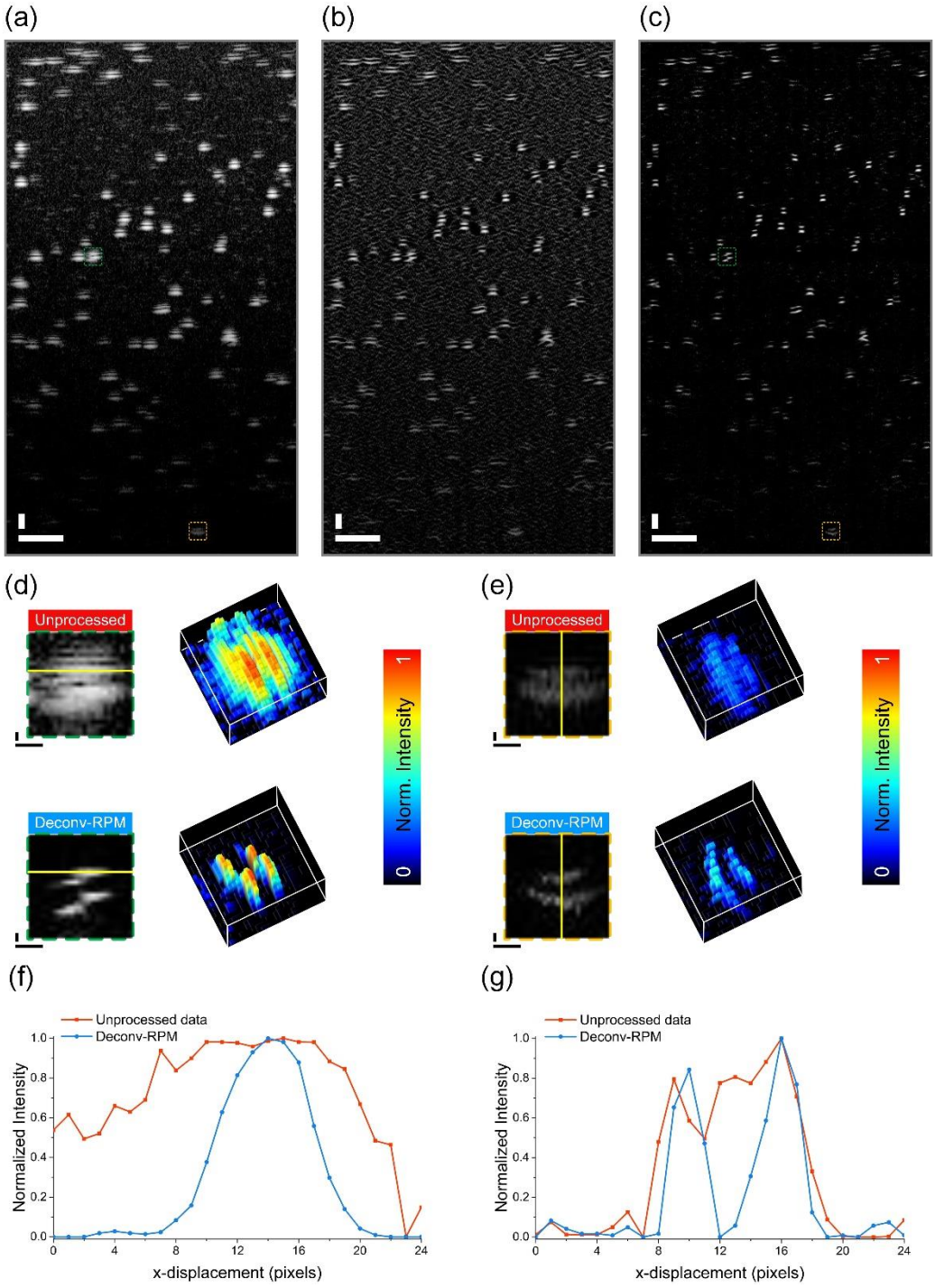

Supplementary Figure 1. Imaging of particles suspension phantom acquired with micro-OCT (a), processed with deconvolution only (b) and Deconv-RPM (c) on logarithmic scale. Scale bars: 10 μm. (d-e) Close-up view (6X) of selected particles near (green dashed-line box) and outside (orange dashed-line box) the confocal region, respective 3-D intensity-surface plots of close-up view on the same display scale are shown on the right side. Scale bars: 1 μm. (f-g) Corresponding profiles (yellow lines in d and e) across the hyper-reflective signals are shown to compare the resolved capability before and

after processing, with a μm-per-pixel ratio of 0.525 in the transverse direction (f) and a μm-per-pixel ratio of 0.173 in the axial direction (g).

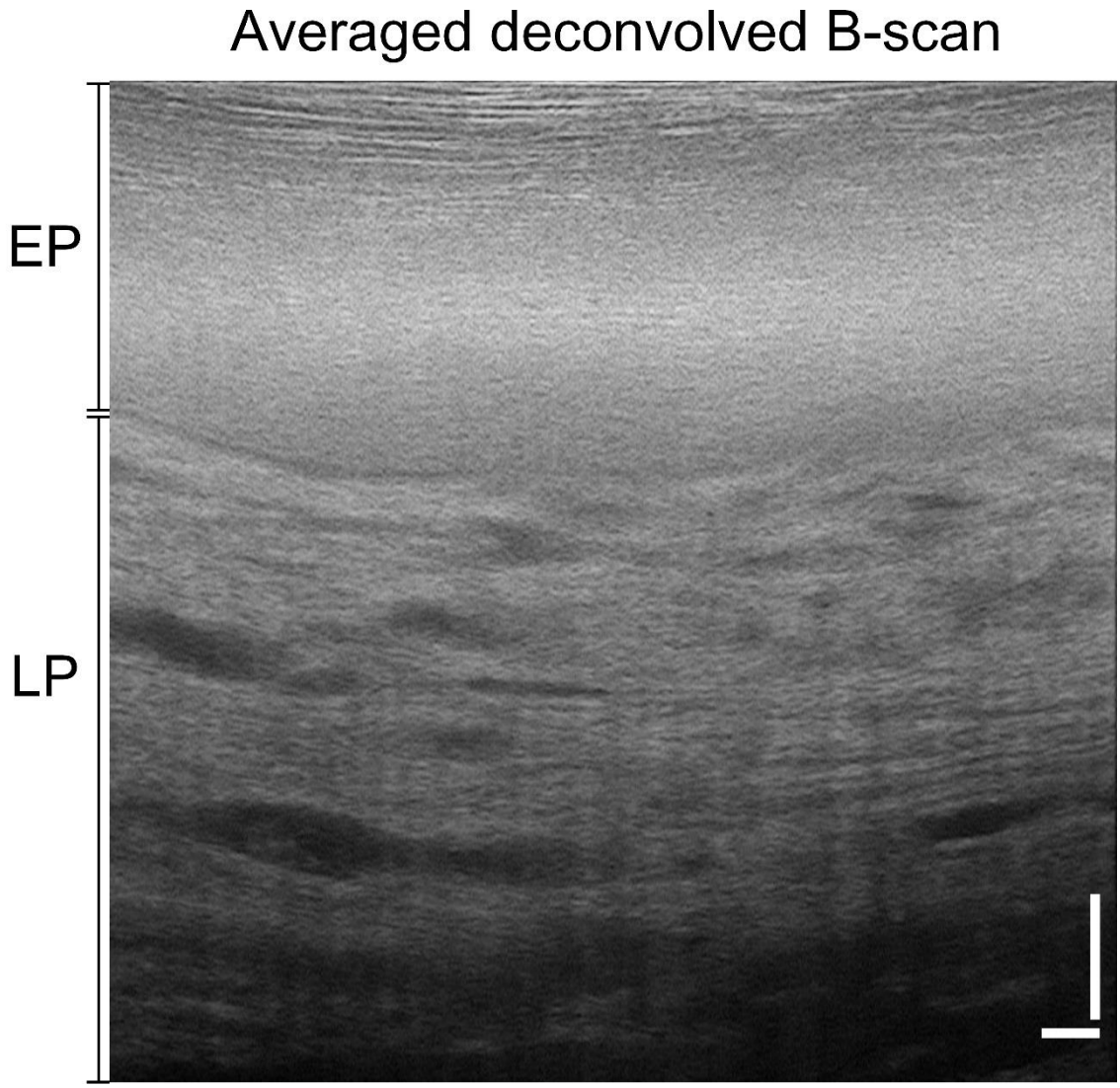

Supplementary Figure 2. Imaging of human labial mucosa with 50 B-scan averages processed by deconvolution only. EP: epithelium, LP: lamina propria. Scale bars, 50 μm.